

Can one hear the shape of a Majorana Billiard?

Barış Pekerten,¹ A. Mert Bozkurt,¹ and İnanç Adagideli¹

¹*Faculty of Engineering and Natural Sciences, Sabancı University, Orhanlı-Tuzla, İstanbul, Turkey*

(Dated: December 15, 2024)

Majorana billiards are finite sized superconductors or semiconductors in proximity to a superconductor, featuring ground state fermion parity switches. We study their “spectra”, i.e. the set of external parameters at which said parity switches occur, and find formulae for the asymptotic mean value of the density of crossings and its oscillations that are analogous to the Weyl expansion and the Gutzwiller trace formula, respectively. Moreover, the statistics of the spacings of parity-crossings are universal and are described by a random matrix ensemble choice of which depends on the antiunitary symmetries of the system in its normal state. We thus demonstrate that “one can hear (information about) the shape of a Majorana billiard” by investigating its spectrum.

Introduction—Eigenvalue spectra of finite quantum systems are related to their shape in the short wavelength limit [1, 2]. The celebrated Weyl expansion relates the smooth part of the density of states (DOS) to the volume, boundary area, curvature and Euler characteristics (number of handles) of the system [2–4]. The remaining part, namely the DOS fluctuations, sensitively depends on the corresponding classical dynamics as well as the type of scattering featured in the system [5–9]. Moreover, if all unitary symmetries are completely broken, the level-spacing distribution becomes universal and reflects the presence or absence of antiunitary symmetries [8, 10–14].

The ground state of conventional, *s*-wave superconductors have an even number of fermions (i.e. even parity), reflecting their completely paired nature. However, under certain conditions, a state with an odd number of fermions (the odd parity state) can cross the even parity state to become the new ground state. This crossing is protected as the level repulsion due to perturbations that mix different fermion parity states are prohibited. While well known within the context of impurity states in superconductors [15], these crossings have attracted recent attention as they are zero dimensional counterparts to topological phase transitions [16–27]. The two states at the transition point are the well known Majorana bound states which feature non-Abelian statistics [28–33]. Although there are strongly suggestive experimental spectral signatures [34–37] of zero bias states, conclusive experimental demonstration of the Majorana bound states has been elusive so far [19, 38–43]. These parity crossings have been regarded as the smoking gun signatures of Majorana states in ballistic 1D wires [44, 45] and their universal statistics were first considered in [20].

In this work, we focus on extracting geometrical information from the set of external parameters at which the ground state fermion parity switches, which we call the “spectra” of parity crossings, in a finite system. Such systems can be either finite sized superconductors or normal-state regions coupled to superconductors (also known as Andreev billiards [46–48]). We call these systems that feature parity switches “Majorana billiards” (MBs). In other words, we ask and answer the question whether

one can “hear” the shape of a Majorana billiard from the “spectra” of parity crossings, alluding to Kac’s famous question, as phrased by L. Bers, “Can one hear the shape of a drum?” [49]. Although isospectral domains of different shapes exist [50], it turns out to be possible to extract geometrical and dynamical information from the energy spectra. We show here how the shape of a Majorana billiard is related to its spectrum of parity crossings by studying the set of external parameters (such as chemical potential or applied magnetic field values) at which the MB’s ground state parity switches. To this end, we first relate the parity crossing values of a MB to the real eigenvalues of another (fictional) non-Hermitian “Hamiltonian”. We thus extend the usual spectral geometric results such as Weyl expansion (Fig. 2), density of states oscillations (Fig. 3) and universal level statistics (Fig. 4 and 5) from its usual context of energy eigenvalues to parity crossings.

Description of the system—We consider finite 2D MB systems whose dynamics are described by the Bogoliubov–de Gennes Hamiltonian [51–53]:

$$H_s = h(p, \mathbf{r}) \tau_z + \alpha(p_x \sigma_y - p_y \sigma_x) \tau_z + B \sigma_x + \Delta \tau_x. \quad (1)$$

Here, σ_i [τ_i] are the Pauli matrices in spin [particle-hole] space with $i = x, y, z$, $h(p, \mathbf{r}) = p^2/2m + V(\mathbf{r}) - \mu$ is the spinless part of the single-particle Hamiltonian with \mathbf{r} a point in the system, α is the spin-orbit interaction (SOI) constant, B is the Zeeman field and Δ is the *s*-wave pairing potential. $V(\mathbf{x})$ is the on-site, single-particle potential which includes disorder and confinement potentials. The systems can be clean or disordered, and their geometry could lead to chaotic or integrable dynamics in the classical limit (Fig. 1). We will also discuss the so-called depleted range of H_s , where the Zeeman field is large enough to deplete one of the spin-split bands [52, 53]. This range is described by the Hamiltonian

$$H_p = h(p, \mathbf{r}) \tau_z + \Delta' \boldsymbol{\tau} \cdot \mathbf{p}, \quad (2)$$

where $\Delta' = \alpha \Delta / \epsilon$ is the effective SOI strength, with $\epsilon = \sqrt{B^2 - \Delta^2}$ for $B > \Delta$. Throughout this manuscript, we call systems featuring H_s (H_p) “*s*-wave” (“*p*-wave”). Both *s*- and *p*-wave systems can support Majorana

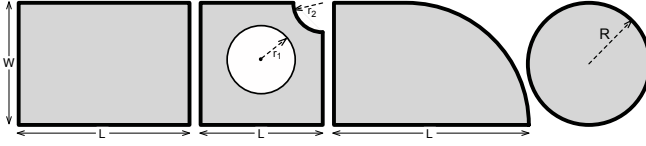


FIG. 1. The 2D geometries considered in the TB numerical simulations: a) Rectangle, b) Lorentz gas cavity, c) Quarter-stadium cavity, d) Disk.

bound states for certain ranges of their external and material parameters, thus allowing for a switch in ground state fermion parity as an external parameter is varied.

Parity crossings for Majorana billiards: Mapping to the Weyl problem— We start by considering the parity crossings of the p -wave Hamiltonian of Eq. (2), as the discussion is simpler. The parity crossing points μ_i are the chemical potential values for which two eigenstates of the p -wave Hamiltonian cross at zero energy, i.e. $H_p|_{\mu=\mu_i} \chi = 0$ for nontrivial χ . We define the density of crossings as $\rho(\mu) = \sum_i \delta(\mu - \mu_i)$, and investigate the asymptotic behavior of $\rho(\mu)$ as well as the related quantity $\mathcal{N}(\mu) = \int_{-\infty}^{\mu} \rho(\mu') d\mu'$, the number of crossing points below μ , for large μ . As is the case for the density of states, we distinguish the average density of crossings $\bar{\rho}$ and its oscillations ρ_{osc} and write $\rho(\mu) = \bar{\rho}(\mu) + \rho_{\text{osc}}(\mu)$ [3–7]. We consider these two terms separately below.

We start by mapping the problem of finding the parity crossing points to that of finding eigenvalues of a non-Hermitian operator by premultiplying Eq. (2) with τ_z :

$$\left(\frac{(\mathbf{p} + im\Delta'\boldsymbol{\eta})^2}{2m} + V(\mathbf{r}) + m\Delta'^2 \right) \chi = \mu \chi, \quad (3)$$

where $\boldsymbol{\eta} = \tau_y \hat{x} - \tau_x \hat{y}$. We identify this operator as the Hamiltonian of a Rashba 2DEG with an imaginary Rashba parameter $\alpha = i\Delta'$. The real eigenvalues of this operator are the crossing points of the original Hamiltonian whereas the complex eigenvalues are associated with avoided crossings. While there is no general reason to assume that a given eigenvalue is real, in the limit of at least one of the system size parameters W (the width, along the direction which we choose to be the y -axis) is much smaller than the coherence length $\xi = \hbar/m\Delta'$, almost all eigenvalues of this operator are real. Rescaling the eigenfunction $\chi = e^{\boldsymbol{\eta} \cdot \mathbf{r}/\xi - r^2/\xi^2} \tilde{\chi}$ and expanding in powers of W/ξ , we obtain [54]

$$\left(\frac{(\mathbf{p} + \frac{2m^2\Delta'^2}{\hbar} (\hat{\mathbf{z}} \times \mathbf{r}) \tau_z)^2}{2m} + V(\mathbf{r}) + m\Delta'^2 \right) \tilde{\chi} = \mu \tilde{\chi}. \quad (4)$$

We see that the crossing points are eigenvalues of the normal state Hamiltonian with fictitious magnetic field $\pm 2m^2\Delta'^2/e\hbar$ and constant potential shift $m\Delta'^2$. We note that the energy levels are even functions of applied magnetic fields. Therefore, to the order we are working in,

the effect of the fictitious magnetic field on the crossing points can be ignored as they only serve to modify the nonzero split in energy levels. We thus arrive at the remarkable result that the values of all parity crossing points are simply energy eigenvalues of the *normal state* Hamiltonian $H_N = p^2/2m + V(\mathbf{r}) + m\Delta'^2$. This identification allows us to map the average density of parity crossings to the conventional density of states of a normal state hamiltonian. Well known results from the asymptotic density of states, namely the Weyl expansion [1–3], or for soft confinement the Thomas-Fermi approximation [4], or for disordered systems the theory of Lifshitz tails [57–59], as well as the random matrix theory results for DOS fluctuations [20, 55] carry over to the spectra of parity crossings.

For the average density of parity crossings for the p -wave system $\bar{\rho}_{w,p}(\mu)$ in d dimensions, we obtain:

$$\bar{\rho}_{w,p}(\mu) = \begin{cases} \frac{L}{2\pi\sqrt{\mu}} + \mathcal{O}(1) & \text{if } d = 1 \\ \frac{S}{4\pi} - \frac{\partial S}{8\pi\sqrt{\mu}} & \text{if } d = 2 \\ \frac{V\sqrt{\mu}}{4\pi^2} - \frac{\partial V}{16\pi} & \text{if } d = 3, \end{cases} \quad (5)$$

where L is the length of the 1D wire, S and ∂S are respectively the area and perimeter of the 2D billiard, and V and ∂V the volume and surface area of the 3D dot cavity respectively. In order to demonstrate our analytical results above for average density, we perform tight-binding simulations of parity crossings in a p -wave MB using the Kwant toolbox [56] for quantum transport (see Appendix A for details). Our results for a 2D Majorana billiard are presented in Fig. 2a and b, where we plot $\mathcal{N}(\mu)$ both as derived from Eq. (5) (dashed lines) and as obtained from the TB simulation (solid, stepped lines). We see that the results fit well once the boundary corrections in Eq. (5) are taken into account. We note that there are no fitting parameters in the analytical plots. For a one dimensional disordered wire, we notice parity crossings in the fully depleted wire caused by rare disorder configurations (Fig. 2c). We identify these as analogous to the states that form the well known Lifshitz tail [57–59]. For the average density formula and further discussion, we refer the reader to Appendix D.

We next consider the case of the s -wave system described by the Hamiltonian H_s in Eq. (1) where we have two external parameters, namely μ and B . We follow Ref. [54, 60] to again transform the usual eigenvalue problem to a non-Hermitian one at zero energy and obtain:

$$(h(p, \mathbf{r})\sigma_z - iap_x\sigma_x \mp B \mp \Delta\sigma_x) \phi_{\pm} = 0. \quad (6)$$

Here, we ignored the chiral symmetry breaking term $iap_y\sigma_y$, which is a valid approximation in the limit $W \ll \xi$. For a finite system, the solution that satisfies all boundary conditions can be expressed in terms of the eigenfunctions of the normal state hamiltonian $h\psi_n = (E_n - \mu)\psi_n$ as

$$\phi_{n,\pm} = \zeta_{\pm} e^{\pm x/\xi} \psi_n, \quad (7)$$

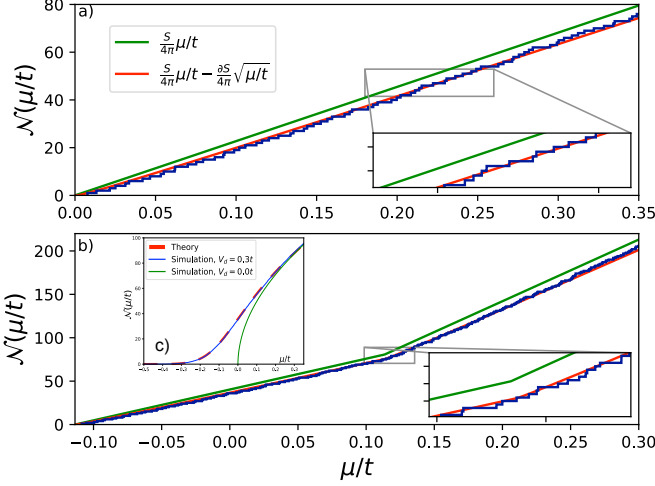


FIG. 2. (Color online) $\mathcal{N}(\mu/t)$ for a ballistic quarter stadium MB (see Fig. 1c). The green line is to the first term in the Weyl expansion whereas the red line includes the surface corrections. The staircase plot is the result of TB simulations. Lower-right insets are zoom-ins to show the fit between TB simulation and theory. a) p -wave MB with $L = 80a$, $W = 40a$ and $\Delta' = 0.001ta$. b) s -wave MB with $L = 100a$, $W = 50a$, $B = 0.23t$, $\Delta = 0.2t$ and $\alpha = 0.001ta$. The kink in the plot is at $\mu = \epsilon$ and signals the entrance of the second spin band into the picture. c) $\mathcal{N}(\mu/t)$ vs μ/t for a disorder averaged (200 realizations) 1D p -wave MB with $L = 500a$ and $\Delta' = 0.001ta$. The theory [58, 59] and the TB simulation results are shown. (See Appendix D for more details.)

where $\zeta_{\pm}(\epsilon)$ are the eigenvectors of the 2×2 matrix $(E_n - \mu)\sigma_z \mp \Delta\sigma_x$ with eigenvalue $\pm\sqrt{(E_n - \mu)^2 + \Delta^2}$. Substituting into Eq. (6), we find that the zero mode solutions (hence the parity crossings) happen on the curves in the $B - \mu$ plane that satisfy

$$B^2 = (\mu - E_n)^2 + \Delta^2, \quad (8)$$

for a given eigenvalue E_n of the spinless single particle Hamiltonian $h(p, \mathbf{r})$. Hence, the density of parity crossing points (either in μ or B) can be obtained by analyzing the set of eigenvalues $\{E_n\}$ of $h(p, \mathbf{r}) - \mu$. Noting that $h(p, \mathbf{r})$ is the same for s - and p -wave cases, we write the s -wave Weyl expansion for $\rho_{w,s}(\mu)$ and $\rho_{w,s}(B)$ for parity crossing densities in terms of their p -wave counterpart $\rho_{w,p}(\mu)$ in Eq. (5):

$$\rho_{w,s}(\mu, B) = \sum_{\varsigma=\pm 1} \rho_{w,p}(\mu + \varsigma\epsilon(B)) \theta(\mu + \varsigma\epsilon(B)). \quad (9)$$

The asymptotic mean spacing $\langle \delta\mu \rangle = \rho_{w,s}^{-1}(\mu)$ or $\langle \delta B \rangle = \rho_{w,s}^{-1}(B)$ between crossing points can be obtained by inverting these expressions.

Oscillations in density of parity crossing points—We next investigate the oscillatory behavior of the density of parity crossings for a p -wave Majorana billiard, due to interference between the actions of periodic semiclassical paths, as described by Gutzwiller's trace formula for

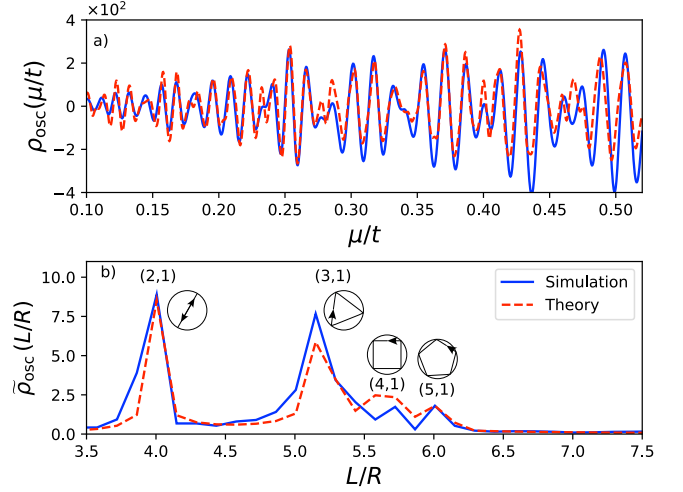


FIG. 3. (Color online) a) Density oscillations of parity crossings ρ_{osc} for a clean p -wave disk MB with $R = 100a$, $\Delta' = 0.001ta$. b) The Fourier transform of ρ_{osc} . The (v, w) pairs and corresponding classical orbits for the peaks are labeled. The smoothing parameter for both figures is $\gamma = 0.4/R$.

billiards [7, 47, 61–63]. We again take advantage of the parity crossing density being given by the normal state Hamiltonian, essentially adapt the discussion in Ref. [4] to the case of the clean p -wave system and obtain its oscillatory part as:

$$\rho_{osc}(\mu) = \frac{2m}{(2\pi\hbar)^{3/2}p} \sum_{po} \mathcal{A}_{po} \cos \left[\frac{1}{\hbar} S_{po}(\mu) - \phi_{po} \right], \quad (10)$$

where the sum is over classical periodic orbits, the amplitude \mathcal{A}_{po} is given by $\mathcal{A}_{po} = \int_{po} |\mathcal{J}_{po}|^{-1/2} dr_{\parallel} dr_{\perp}$, S_{po} is the classical action over the orbit in question and $\phi_{po} = \sigma_{po}\pi/2 + \pi/4$ is the associated phase of the orbit with σ_{po} as the Maslov index. r_{\parallel} (r_{\perp}) are the coordinates parallel (perpendicular) to the orbit, and $\mathcal{J}_{po} = (\partial r_{\perp}/\partial p'_{\perp})_{po}$ quantifies the stability of the orbit with initial momentum \mathbf{p}' and final position \mathbf{r} considering only perturbations perpendicular to the trajectory.

We now exemplify this result by considering a clean disk p -wave MB and compare the theory to TB simulations. (See Appendix C for the adaptation of Eq. (10) to a 2D TB disk MB.) In Fig. 3a, we plot the oscillatory part of the density of parity crossings ($\rho_{osc}(\mu)$) as a function of μ , as derived by Gutzwiller's trace formula and as given by our numerical simulations and show that the results fit well (without any fitting parameters). (Both the simulation results and the theory are smoothed using a Gaussian.) In Fig. 3b, we plot the Fourier transform of the above plot ($\tilde{\rho}_{osc}(L/R)$ where L is the length of the orbit and R is the radius of the disk). We identify the peaks in this plot corresponding to the lengths of the classical periodic orbits $L_{vw} = 2\pi R \sin(\varphi_{vw})$, where $\varphi_{vw} \equiv \pi w/v$ and the two integers v, w are the number of vertices and windings of the orbit, respectively.

Universal fluctuation statistics of parity crossing spacings— We now focus on how the parity crossings are correlated. If at least one of the system size parameters (the “width”) becomes smaller than the coherence length, we find that the distribution of spacings, while universal, depends on whether the underlying normal system is regular, diffusive, chaotic or localized [20, 55]. For crossing spacings smaller than the normal state Thouless energy, the parity crossing points are described by an ensemble of real Hermitian random matrices, namely the orthogonal ensemble. The corresponding distribution of crossing spacings is given by the Wigner-Dyson distribution [8, 10–13]. Hence, the probability density $P(\delta\mu)$ associated with obtaining a crossing spacing of $\delta\mu$ is:

$$P(\delta\mu) = \frac{\pi\delta\mu}{2\langle\delta\mu\rangle} \exp\left(-\frac{\pi\delta\mu^2}{4\langle\delta\mu\rangle^2}\right) \quad (11)$$

When the mean crossing spacing is much bigger than the Thouless energy, the normal state is localized and the level spacing distribution is Poissonian:

$$P(\delta\mu) = \exp(-\delta\mu/\langle\delta\mu\rangle). \quad (12)$$

When the localization length is comparable to the system size, the normal state system is near the Anderson phase transition, the states are forced to overlap, leading to linear level repulsion for small spacings that turn into an exponential tail for larger energy spacings [20, 55], signaling the fractal structure of the Majorana wavefunction:

$$P(\delta\mu) = \frac{\delta\mu}{\langle\delta\mu\rangle} \exp(-2\delta\mu/\langle\delta\mu\rangle). \quad (13)$$

We again simulate these cases with a TB model and plot the results against the probability distribution functions in Eq. (11), (12) and (13). Fig. 4 (Fig. 5) shows our *p*-wave (*s*-wave) results for disordered rectangle cavities (a-c) and chaotic billiards (d). In line with the above prediction, the distributions evolve from Wigner-Dyson to semi-Poissonian to Poissonian as the system goes from localized to diffusive, and fit the respective distributions well without any fitting parameters (see Fig. 4 and Appendix A). We note, however, that in the *s*-wave case, $P(\delta\mu \rightarrow 0)$ approaches 0.5 if both spin species are populated. This is understood by considering the parity crossing points as two interlaced sequences belonging to different spin species for larger B [60]. The elements of each sequence feature level repulsion, and one sequence is the same as the other sequence, but shifted (by the Zeeman energy). For large enough shifts two sequences gets uncorrelated suppressing the level repulsion between half the levels. This leads to the value 0.5 for the spacing distribution function at zero.

In conclusion, we show that the set of external parameters at which the ground state fermion parity of a Majorana billiard switches (the “spectrum” of the MB) is subject to well-known asymptotic analysis of eigenvalues of the Laplacian operator having disorder or chaotic dynamics. In particular, we show that the mean density of

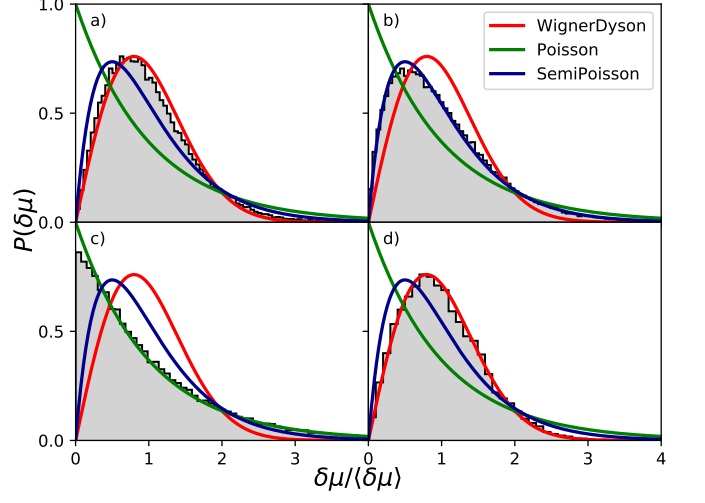


FIG. 4. (Color online) a-c) Level spacing distributions for a disordered rectangular *p*-wave MBs of varying lengths, averaged over 500 disorder realizations, with $\Delta' = 0.025ta$, disorder strength $V_d = 0.5t$, width $W = 20a$. a) $L = 40a = \xi$, b) $L = 100a \gtrsim \xi$ and c) $L = 1600a \gg \xi$, with ξ being the coherence length. d) Level spacing distributions, averaged over 225 cavity realizations, for a clean *p*-wave Lorentz cavity MB. Here, $\Delta' = 10^{-3}ta$, $L = 50a$, $W = 50a$, and $r1 = r2 = 10a$.

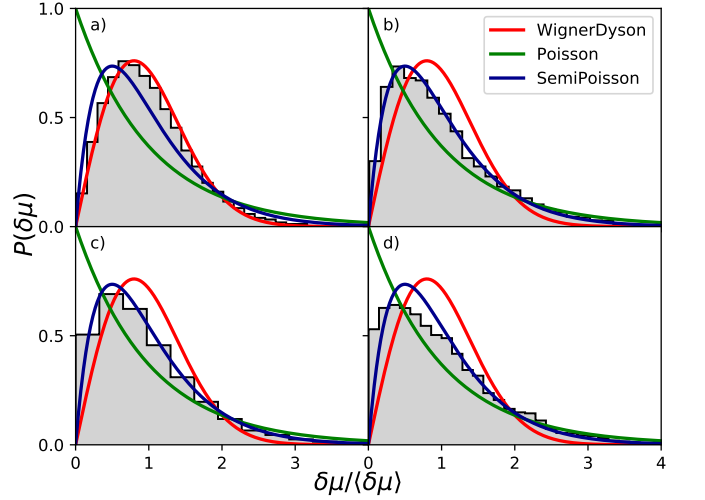


FIG. 5. (Color online) a-c) Level spacing distributions for disordered rectangular *s*-wave MBs with increasing Zeeman energy B , averaged over 500 disorder realizations, with $L = 200a$, $W = 10a$, $V_d = 0.2t$, $\alpha = 0.025ta$, $\Delta = 0.12t$, and a) $B = 1.12t$, b) $B = 0.22t$ and c) $B = 0.13t$. d) Level spacing distributions for clean *s*-wave Lorentz cavity MB, averaged over 225 cavity realizations. Here, $\alpha = 0.001ta$, $\Delta = 0.2t$, $B = 0.23t$, $L = 50a$, $W = 50a$, and $r1 = r2 = 10a$.

crossings obey a Weyl expansion, and has a Lifshitz tail in the disordered case. Moreover, we demonstrate that the oscillations of the density of parity crossings can be obtained by semiclassical means extending Gutzwiller’s trace formula to Majorana billiards. Finally, we show that the spacing fluctuations of parity switches obey a

universal distribution, as described by random matrix theory. We thus demonstrate that “one can hear (information about) the shape of a Majorana billiard.”

Acknowledgments— We thank M. Wimmer, K. Richter and C.W.J. Beenakker for useful discussions. This work

was supported by funds of the Erdal İnönü chair. İ.A. is a member of the Science Academy–Bilim Akademisi–Turkey; B.P. and A.M.B thank the Science Academy–Bilim Akademisi–Turkey for the use of their facilities throughout this work.

[1] H. Weyl and K. Chandrasekharan *Gesammelte Abhandlungen I*, v.4 (Springer Berlin Heidelberg, 1968)

[2] H. Baltes and E. Hilf, *Spectra of finite systems: a review of Weyl's problem, the eigenvalue distribution of the wave equation for finite domains and its applications on the physics of small systems* (Bibliographisches Institut, 1976)

[3] R. Balian and C. Bloch, *Annals of Physics* **60**, 401 (1970)

[4] M. Brack and R. K. Bhaduri, *Semiclassical Physics*, (Westview, Boulder, Colo., 2003)

[5] R. Balian and C. Bloch, *Annals of Physics* **69**, 76160 (1972)

[6] M. V. Berry, *Proc. R. Soc. of London. Series A, Mathematical and Physical Sciences* **400**, 229 (1985).

[7] M. C. Gutzwiller, *Chaos in Classical and Quantum Mechanics*, (Springer, New York, 1990)

[8] M. Mehta, *Random Matrices*, Pure and Applied Mathematics (Elsevier Science, 2004)

[9] J. Wurm, A. Rycerz, İ. Adagideli, M. Wimmer, K. Richter, and H. U. Baranger, *Phys. Rev. Lett.* **102**, 056806 (2009).

[10] E. P. Wigner, *Annals of Mathematics* **62**, 548 (1955)

[11] F. J. Dyson, *Journal of Mathematical Physics* **3**, 1199 (1962)

[12] F. J. Dyson, *Journal of Mathematical Physics* **3**, 157165 (1962)

[13] F. J. Dyson and M. L. Mehta, *Journal of Mathematical Physics* **4**, 701712 (1963)

[14] O. Bohigas, M. J. Giannoni, and C. Schmit, *Phys. Rev. Lett.* **52**, 1 (1984)

[15] A. V. Balatsky, I. Vekhter, and J.-X. Zhu, *Rev. Mod. Phys.* **78**, 373 (2006)

[16] L. Fu and C. L. Kane, *Physical Review B* **79** (2009)

[17] S. Ryu, A. P. Schnyder, A. Furusaki, and A. W. W. Ludwig, *New Journal of Physics* **12**, 065010 (2010)

[18] T. D. Stanescu, R. M. Lutchyn, and S. Das Sarma, *Phys. Rev. B* **84**, 144522 (2011)

[19] E. J. H. Lee, X. Jiang, R. Aguado, G. Katsaros, C. M. Lieber, and S. De Franceschi, *Phys. Rev. Lett.* **109**, 186802 (2012)

[20] C. W. J. Beenakker, J. M. Edge, J. P. Dahlhaus, D. I. Pikulin, S. Mi, and M. Wimmer, *Phys. Rev. Lett.* **111**, 037001 (2013)

[21] M.-T. Rieder, P. W. Brouwer, and İ. Adagideli, *Phys. Rev. B* **88**, 060509 (2013)

[22] W. Chang, V. E. Manucharyan, T. S. Jespersen, J. Nygård, and C. M. Marcus, *Phys. Rev. Lett.* **110**, 217005 (2013)

[23] J. D. Sau and E. Demler, *Phys. Rev. B* **88**, 205402 (2013)

[24] D. M. Badiane, L. I. Glazman, M. Houzet, and J. S. Meyer, *Comptes Rendus Physique* **14**, 840856 (2013)

[25] D. Chevallier, P. Simon, and C. Bena, *Phys. Rev. B* **88**, 165401 (2013)

[26] E. J. H. Lee, X. Jiang, M. Houzet, R. Aguado, C. M. Lieber, and S. De Franceschi, *Nat. Nano.* **9**, 79 (2014)

[27] S. Hegde, V. Shivamoggi, S. Vishveshwara, and D. Sen, *New J. Phys.* **17**, 053036 (2015).

[28] A. Y. Kitaev, *Physics-Uspekhi* **44**, 131 (2001)

[29] M. Z. Hasan and C. L. Kane, *Rev. Mod. Phys.* **82**, 3045 (2010)

[30] X.-L. Qi and S.-C. Zhang, *Rev. Mod. Phys.* **83**, 1057 (2011)

[31] J. Alicea, *Reports on Progress in Physics* **75**, 076501 (2012)

[32] B. A. Bernevig and T. Hughes *Topological Insulators and Topological Superconductors* (Princeton University Press, 41 William Street, Princeton, New Jersey 08540, 2013)

[33] S. R. Elliott and M. Franz, *Rev. Mod. Phys.* **87**, 137 (2015)

[34] V. Mourik, K. Zuo, S. M. Frolov, S. R. Plissard, E. P. A. M. Bakkers and L. P. Kouwenhoven, *Science* **336**, 1003 (2012)

[35] S. Nadj-Perge, I. K. Drozdov, J. Li, H. Chen, S. Jeon, J. Seo, A. H. MacDonald, B. A. Bernevig and A. Yazdani, *Science* **346**, 602 (2014)

[36] A. Fornieri, A. M. Whiticar, F. Setiawan, E. P. Marín, A. C. C. Drachmann, A. Keselman, S. Gronin, C. Thomas, T. Wang, R. Kallaher, G. C. Gardner, E. Berg, M. J. Manfra, A. Stern, C. M. Marcus, and F. Nichele, *arXiv:1809.03037* (2018).

[37] S. Vaitiekėnas, M.-T. Deng, P. Krogstrup, and C. M. Marcus, *arXiv:1809.05513* (2018).

[38] E. Prada, P. San-Jose, and R. Aguado, *Phys. Rev. B* **86**, 180503 (2012)

[39] J. Liu, A. C. Potter, K. T. Law, and P. A. Lee, *Phys. Rev. Lett.* **109**, 267002 (2012)

[40] D. Bagrets and A. Altland, *Phys. Rev. Lett.* **109**, 227005 (2012)

[41] D. I. Pikulin, J. P. Dahlhaus, M. Wimmer, H. Schomerus, and C. W. J. Beenakker, *New Journal of Physics* **14**, 125011 (2012)

[42] H. O. H. Churchill, V. Fatemi, K. Grove-Rasmussen, M. T. Deng, P. Caroff, H. Q. Xu, and C. M. Marcus, *Phys. Rev. B* **87**, 241401 (2013)

[43] C.-X. Liu, J. D. Sau, and S. Das Sarma, *Physical Review B* **97** (2018)

[44] S. Das Sarma, J. D. Sau, and T. D. Stanescu, *Phys. Rev. B* **86**, 220506 (2012)

[45] R. Rodríguez-Mota, S. Vishveshwara, and T. Pereg-Barnea, *J. Phys. Chem. Solids* (2018)

[46] I. Kosztin, D. L. Maslov, and P. M. Goldbart, *Phys. Rev. Lett.* **75**, 1735 (1995).

[47] I. Adagideli and P. M. Goldbart, *Int. J. Mod. Phys. B* **16**, 1381 (2002)

[48] C. W. J. Beenakker, in *Quantum Dots: A Doorway to Nanoscale Physics*, edited by W. Dieter Heiss (Springer Berlin Heidelberg, Berlin, Heidelberg, 2005), pp. 131174.

[49] M. Kac, *The American Mathematical Monthly* **73**, 1

(1966)

[50] C. Gordon, D. Webb, and S. Wolpert, *Invent. Math.* **110**, 1 (1992).

[51] P. G. deGennes, *Superconductivity of Metals and Alloys* (Westview Press, 1999)

[52] R. M. Lutchyn, J. D. Sau, and S. Das Sarma, *Phys. Rev. Lett.* **105**, 077001 (2010)

[53] Y. Oreg, G. Refael, and F. von Oppen, *Phys. Rev. Lett.* **105**, 177002 (2010)

[54] İ. Adagideli, M. Wimmer, and A. Teker, *Phys. Rev. B* **89**, 144506 (2014)

[55] C. W. J. Beenakker, *Rev. Mod. Phys.* **69**, 731 (1997)

[56] C. W. Groth, M. Wimmer, A. R. Akhmerov, and X. Waintal, *New Journal of Physics* **16**, 063065 (2014)

[57] I. M. Lifshitz, *Advances in Physics* **13**, 483 (1964).

[58] B. I. Halperin, *Phys. Rev.* **139**, A104 (1965).

[59] C. Itzykson and J.-M. Drouffe, *Statistical Field Theory* v.2 (Cambridge University Press, Cambridge [England]; New York, 1989).

[60] B. Pekerten, A. Teker, O. Bozat, M. Wimmer, and İ. Adagideli, *Phys. Rev. B* **95**, 064507 (2017)

[61] R. A. Jalabert, H. U. Baranger, and A. D. Stone, *Phys. Rev. Lett.* **65**, 2442 (1990).

[62] H. Ishio and J. Burgdörfer, *Phys. Rev. B* **51**, 2013 (1995).

[63] İ. Adagideli and P. M. Goldbart, *Phys. Rev. B* **65**, (2002).

[64] S. Datta, *Electronic Transport in Mesoscopic Systems* (Cambridge University Press, 1997)

[65] E. Jones, E. Oliphant, P. Peterson et al. **SciPy: Open Source Scientific Tools for Python** (2001-
<http://www.scipy.org/> [Online; accessed 2018-04-01].

Appendix A: Numerical calculation of the parity crossing points using tight-binding approximation

For the p -wave numerical results, we start with the LHS of Eq. (3), which is a non-Hermitian operator, as opposed to the p -wave Hamiltonian in Eq. (2). This non-Hermitian operator and the p -wave Hamiltonian are equivalent in the sense that no approximation was made in going from Eq. (2) to Eq. (3). We form the tight-binding (TB) form of this operator using conventional methods (see, for example, [64]):

$$\hat{O}_{\text{TB}}^{\text{PW}} = (2dt + V(x, y)) \tau_0 |x, y\rangle \langle x, y| - t\tau_0 [|x + a, y\rangle \langle x, y| + |x, y + a\rangle \langle x, y| + \text{h.c.}] + i\Delta' \left[\frac{i}{2}\tau_y |x + a, y\rangle \langle x, y| + \frac{i}{2}\tau_x |x, y + a\rangle \langle x, y| + \text{h.c.} \right], \quad (\text{A1})$$

where $t = \hbar^2/2ma^2$ is the hopping parameter, a is the lattice constant for the TB lattice and $V(x, y)$ is the onsite potential. For disordered systems, we take the disorder to be Gaussian, i.e. $\langle V(\mathbf{r})V(\mathbf{r}') \rangle = D\delta(\mathbf{r} - \mathbf{r}')$ for \mathbf{r}, \mathbf{r}' within the system, where $\langle \dots \rangle$ represents averaging over disorder realizations, $D \equiv V_d^2 a^d$ with V_d is the disorder strength and d is the dimension of the system ($d = 2$ in most of our manuscript; if $d = 1$, then the hoppings in the y -direction are absent). in TB simulations, this

corresponds to choosing randomly the on-site potential from a Gaussian distribution. For ballistic cavity results, we set $V(x, y) = 0$ within the cavity. The boundaries of the system are defined by the lack of hopping to outside. We form the TB sparse matrix of this operator using the Kwant library [56] over the system shape which described in Fig. 1 and the relevant plots. We then numerically obtain the eigenvalues of this (non-Hermitian) sparse matrix using LAPACK libraries present in the SciPy package [65]. We finally discard non-real eigenvalues to obtain our results.

For the s -wave results, we go through the same procedure, except for utilizing the appropriate TB-representation of the non-Hermitian operator derived from the Hamiltonian in Eq. (1). For $E = 0$, the TB model for the s -wave equivalent of Eq. (3) reads $\hat{O}_{\text{TB}}^{\text{SW}}\chi = \mu\chi$, with the non-Hermitian operator $\hat{O}_{\text{TB}}^{\text{SW}}$ defined as:

$$\begin{aligned} \hat{O}_{\text{TB}}^{\text{SW}} = & [(2dt + V(x, y)) \sigma_0 \tau_0 + B \sigma_x \tau_z] |x, y\rangle \langle x, y| \\ & - t\sigma_0 \tau_0 [|x + a, y\rangle \langle x, y| + |x, y + a\rangle \langle x, y| + \text{h.c.}] \\ & - \sigma_y \tau_0 \left[\frac{i\alpha}{2} |x + a, y\rangle \langle x, y| + \text{h.c.} \right] \\ & + \sigma_x \tau_0 \left[\frac{i\alpha}{2} |x, y + a\rangle \langle x, y| + \text{h.c.} \right] \\ & + i\Delta\sigma_0 \tau_y |x, y\rangle \langle x, y|. \end{aligned} \quad (\text{A2})$$

Again, in the plots where $d = 1$, the hopping in the y -direction are absent.

For disorder averaging, we create many realizations of the same disordered system and do statistics over the combined results of each realization. For shape averaging over chaotic cavities, we create many realizations of the same chaotic cavity, the difference between realizations being the positioning of a relevant geometrical feature of the cavity, without changing the size of the system volume or boundary. For the Lorentz cavity, for example, we slightly change the position of the central stopper for each realization (making sure the stopper never comes too close to a wall). We make sure the change is large enough numerically to yield a completely different set of eigenvalues.

Appendix B: Universal spectra of parity crossing points in s -wave systems

In this section, we note that for a given disorder realization in a given s -wave system, the placement of the parity crossing points as a function of $\mu + \sqrt{B^2 - \Delta^2}$ is universal as other system parameters are varied, as indicated in Eq. (8). In Fig. 6, we plot the first four eigenvalues of an s -wave system with a specific disorder realization for different values of μ and Δ as a function of B in Fig. 6(a) and as a function of $\mu + \sqrt{B^2 - \Delta^2}$ in Fig. 6(b). We see that in the latter case, all crossings happen at the same points for all parameters. Another salient point seen in Fig. 6 is that the particle-hole symmetry assures another

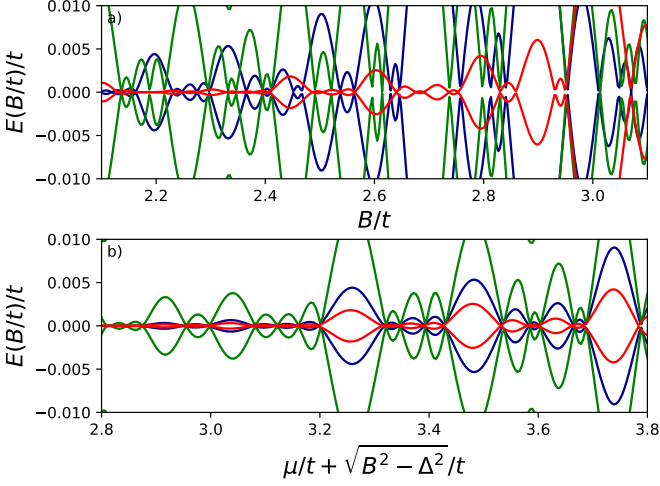


FIG. 6. (Color online) A plot of the lowest four eigenvalues of the disordered s -wave Hamiltonian in Eq. (1), discretized on a 1D lattice of 100 sites, plotted as a function of (a) B/t and (b) $\mu/t + \sqrt{B^2 - \Delta^2}/t$, for different values of Hamiltonian parameters. In both plots, the green set of curves represents the lowest four eigenvalues obtained for $\Delta = 1.5t$, $\alpha = 0.05ta$, $\mu = 1.8t$; the blue set is for $\Delta = 1.8t$, $\alpha = 0.05ta$, $\mu = 2.0t$; and the red set is for $\Delta = 1.8t$, $\alpha = 0.08ta$, $\mu = 1.6t$. Here, $t = \hbar^2/2ma^2$ is the hopping parameter. In all cases, the same disorder realization with a disorder strength $V_d = 0.5t$ is taken.

state will cross zero at the same point; level repulsion does not occur because of this symmetry.

Appendix C: Oscillatory behavior of the density of parity crossings on a disk Majorana billiard

In this Appendix, we derive the oscillatory part of the density of parity crossings for a p -wave system on a two dimensional disk MB lattice of radius R , due to the action of the high-symmetry periodic orbits according to Gutzwiller's trace formula [4, 7]. We adapt the continuum version of the 2D disk billiard solutions to our TB simulations in order to show a better fit between theory and simulation. In the TB case, we obtain the classical action of a given orbit from the lattice Hamiltonian $H_{lat} = 2t(1 - \cos(pa/\hbar))$ as

$$S_{vw} = \left(p - \frac{\hbar}{a} \tan\left(\frac{pa}{2\hbar}\right) \right) L_{vw}, \quad (C1)$$

where $L_{vw} = 2vR \sin(\varphi_{vw})$ is the classical orbit length, $\varphi \equiv \pi w/v$ is half of the polar angle and p is the momentum of the particle. v, w are two integers which correspond to the number of vertices and windings of the classical orbit in question, respectively. The oscillatory part $\nu_{osc}(E)$ of the density of states $\rho(E)$ at a given en-

ergy is given as [4]:

$$\rho_{osc}(E) = \frac{1}{E_0} \sqrt{\frac{\hbar}{\pi p R}} \sum_{w=1}^{\infty} \sum_{v=2w}^{\infty} f_{vw} \frac{\sin^{3/2}(\varphi_{vw})}{\sqrt{v}} \times \text{Im} \left[\exp \left\{ i(S_{vw}/\hbar - 3v\pi/2 + 3\pi/4) \right\} \right], \quad (C2)$$

with

$$f_{vw} = \begin{cases} 1 & \text{if } v = 2w \\ 2 & \text{if } v > 2w \end{cases} \quad (C3)$$

and $E_0 \equiv \hbar^2/(2mR^2)$.

For the TB case, we start from $h(p, \mathbf{r})$ of Eq. (2) with $V(\mathbf{r}) = 0$. Then, the TB version of the momentum is given by

$$p(E, \mu) = \frac{\hbar}{a} \arccos \left(1 - \frac{E + \mu}{2t} \right), \quad (C4)$$

where E labels the energy levels of the system. We now use the fact that the parity crossing points μ_c are the eigenvalues of the normal state Hamiltonian and obtain the oscillatory part of the density of parity crossings:

$$\rho_{osc}(\mu) = \frac{1}{E_0} \left(\frac{\hbar}{\pi R p(0, \mu)} \right)^{1/2} \sum_{w=1}^{\infty} \sum_{v=2w}^{\infty} f_{vw} \frac{\sin^{3/2}(\varphi_{vw})}{\sqrt{v}} \times \text{Im} \left[\exp \left\{ iL_{vw} \left(\frac{p(i\gamma, \mu)}{\hbar} - \frac{1}{a} \tan \frac{p(i\gamma, \mu)a}{2\hbar} \right) + i(-3v\pi/2 + 3\pi/4) \right\} \right]. \quad (C5)$$

Here, we combined Eq. (C1), (C2) and (C4) at $E = 0 + i\gamma$, with γ being the smoothing parameter.

To obtain the numerical ρ_{osc} and $\tilde{\rho}_{osc}$ plots in Fig. 3, we set up the TB p -wave system on a circle and obtain the parity crossing points μ_c using the Kwant toolbox as described in the above Appendix section. We then obtain the oscillatory part of the smoothed density ρ_{osc} as

$$\rho_{\gamma}(\mu/t) = \int d\mu' \sum_{\mu_c} \delta(\mu' - \mu_c) F\left(\frac{\mu - \mu'}{\gamma}\right) \rho_{osc}(\mu/t) = \rho_{\gamma}(\mu/t) - \rho_w(\mu/t) \quad (C6)$$

where $F\left(\frac{\mu - \mu'}{\gamma}\right)$ is the smoothing function, which we choose to be Gaussian, γ is the smoothing parameter (the width of the Gaussian), ρ_{γ} is the smooth part of the density of parity crossings and ρ_w corresponds to the volume and surface terms of the Weyl expansion in Eq. (5). We then take the Fourier transform of $\rho_{osc}(k(\mu/t)a) \xrightarrow{\text{FT}} \tilde{\rho}_{osc}(L/R)$ to identify the peaks corresponding to the lowest length L and the highest symmetry semiclassical periodic orbits [4] and plot the results in Fig. 3b.

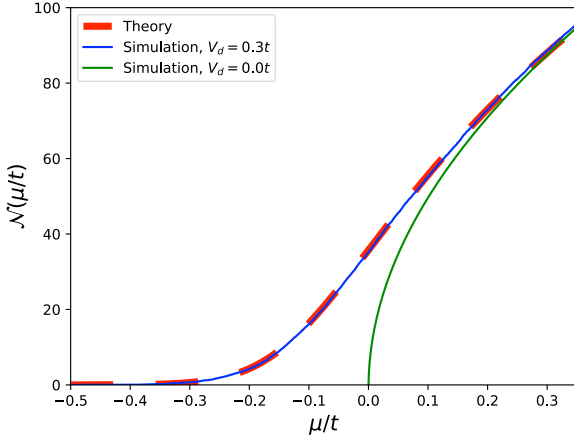


FIG. 7. (Color online) $\mathcal{N}(\mu/t)$ vs. μ/t for a 1D p -wave 1D MB for a wire of length $500a$ and $\Delta' = 0.001ta$. For the disordered case, the TB simulation plot is the average of 200 realizations. The theory lines are the plots of Eq. (D1) for $V_d = 0.0t$ and $V_d = 0.3t$. No fitting parameters are used.

Appendix D: Lifshitz tail in disordered Majorana billiards

Disordered systems feature states below zero energy due to the presence of islands with an average of below zero potential, even though the average potential for the whole system is zero. Called the Lifshitz tail [57], this phenomenon is present also in Majorana billiards (see Fig. 7). The overall disorder-averaged integrated density of parity crossings for a 1D p -wave MB with Gaussian disorder $\langle V(\mathbf{r})V(\mathbf{r}') \rangle = D\delta(\mathbf{r} - \mathbf{r}')$ is given by the formula [58, 59]:

$$\mathcal{N}(\mu) = \frac{\kappa_0}{\pi^2 \varepsilon_0} \frac{1}{[\text{Ai}(-2\mu/\varepsilon_0)]^2 + [\text{Bi}(-2\mu/\varepsilon_0)]^2}, \quad (\text{D1})$$

where Ai and Bi are the Airy functions, $\varepsilon_0 = (D^2 m \hbar^{-2})^{1/3}$ and $\kappa_0 = (D m^2 \hbar^{-4})^{1/3}$.

In Fig. 7, we plot Eq. (D1) and TB simulations for a disordered system (and a clean TB system for comparison). We note that the theory and the numerical simulations fit very well without any fitting parameters.